Computational Aspects of Incrementally Objective Algorithms for Large Deformation Plasticity

Jacob Fish and Kamlun Shek
Departments of Civil, Mechanical and Aerospace Engineering
Rensselaer Polytechnic Institute
Troy, NY 12180, USA

Abstract

A methodology for computationally efficient formulation of the tangent stiffness matrix consistent with incrementally objective algorithms for integrating finite deformation kinematics and with closest point projection algorithms for integrating material response is developed in the context of finite deformation plasticity. Numerical experiments illustrate an excellent performance of the proposed formulation in comparison with other algorithms.

Key Words: Finite Deformation, Plasticity, Objectivity, Consistent Tangent

1.0 Introduction

The notion of consistency between the tangent stiffness matrix and the integration algorithm employed in the solution of the incremental problem has been introduced by Nagtegaal [1] and Simo and Taylor [4]. Within the framework of closest point projection algorithms [2], [5], [6] and in the context of small deformation plasticity, Simo and Taylor [4] demonstrated the crucial role of the consistent tangent stiffness matrix in preserving the quadratic rate of asymptotic convergence of iterative solution schemes based upon the Newton method. Consistent formulations have been subsequently developed for finite deformation plasticity [7], [8], [11] within the framework of multiplicative decomposition of the deformation gradient and hyperelasticity.

It is commonly perceived that the tangent stiffness matrix consistent with the incrementally objective algorithms for integrating finite deformation kinematics and with implicit algorithms for integrating material response is absolutely necessary to optimize the overall computational cost. This notion stems from the common perception that the overall CPU

time in implicit methods is governed by the cost of solving a linearized system of equations. This is certainly true in the asymptotic range in the case of skyline direct solvers ($CPU \propto NB^2$; N, B being the problem size and the bandwidth), multifrontal methods [14] ($CPU \propto N^\beta$, $\beta = 1.2 - 1.7$) and preconditioned conjugate gradient methods [15] ($CPU \propto N^\beta$, $\beta = 1.17 - 1.33$). Multilevel methods, on the other hand, possess an optimal rate of convergence ($\beta=1$), i.e., CPU time is proportional to the number of discrete unknowns. When multilevel methods are employed as linear solvers within the Newton method, the computational complexity of solving a linearized system of equations becomes comparable to that of stiffness matrix evaluation. Table 1 compares the cost of stiffness matrix evaluation with the cost of solving a linear system of equation [17] for several industry and model problems.

TABLE 1. CPU time for stiffness matrix evaluation and solution of linear system of equations

Problem	Element type	Equations	CPU (s) SUN ULTRA SPARC	
			Stiffness Eval	Linear Solver
Turbine Blade [17]	Tetra - 10	207,840	380	820
Ring-Strut [17]	Tetra - 4	102,642	61	126
Turbine Nozzle [17]	Tetra - 10	131,565	212	462
Joint of Cyl. [18]	ANS - 8 [19]	186,245	492	517
Concrete Canoe [17]	ANS - 8 [19]	132,486	390	497
Automobile [17]	DMT-DKT [20]	265,128	395	1116
Hybrid Car [22]	HANS (p=6) [21]	67,120	1850	980

It can be seen that for linear problems solved with multilevel methods [17], [22], the cost of stiffness evaluation ranges from 40% to 190% of the cost of solving a linear system of equations. Note that the cost of element stiffness matrix evaluation has been shown to be proportional to p^4 (p being the polynomial order) for 2D problems [23].

For problems with geometric and material nonlinearities the relative cost of matrix computations is significantly larger. Thus, in the realm where the computational complexity of multilevel solvers is comparable to that of matrix evaluation, stress integration and consistent linearization procedures could potentially become a bottle neck in implicit computations. For large deformation plasticity the following solution strategies are commonly employed:

1. Large increments, consistent tangent [7], [24], [27]

2. Large increments, approximate tangent [25], [26]

3. Small increments, approximate tangent [12]

Each of the three strategies has certain advantages and disadvantages. The first strategy advocating "consistent linearization at any cost" has the advantage of maintaining quadratic asymptotic rate of convergence while advancing solution in large increments. On the negative side, the cost of stress updates and consistent tangent evaluation may often overshadow the entire computational cost in particular in the context of multilevel solvers. The second strategy attempts to reduce the cost of matrix evaluations while advancing the solution in large increments at the expense of suboptimal rate of convergence and consequently increased number of iterations. The third strategy is based on reducing the number of iterations within an increment by employing smaller load steps with approximate and inexpensive tangent, but at the cost of increasing the number of load steps.

The approach advocated here is based on selecting both the simple and accurate integrator [3] that can be consistently linearized to provide a closed form computationally inexpensive tangent stiffness matrix. We show that for moderately large rotation increments the second order accurate incrementally objective integrator [3] is comparable in terms of accuracy to the higher order integrator [26] and at the same time the overall computational cost is drastically reduced in comparison with approaches employing similar integrators but with inconsistent tangents [12].

The manuscript is organized as follows. Section 2 summarizes constitutive equations of finite deformation plasticity based on objective stress rates, additive split of rate of deformation, and associative flow rule. Attention is restricted to materials, such as metals, for which the notion of hypoelasticity is valid. Integration schemes based on the Hughes-Winget incrementally objective algorithm and the closest point projection algorithm [2], [5] originally proposed by Wilkins [6] are then briefly outlined in Section 3. In Section 4 we present a systematic approach for derivation of the tangent stiffness matrix consistent with the integration schemes outlined in Section 3. A number of numerical examples, illustrating the excellent performance of the proposed formulation and comparing it with ABAQUS [12], complete the manuscript.

2.0 Rate constitutive equations

The following notation is employed: the left superscript denotes the configuration, such that $^{t+\Delta t}\square$ denotes the current configuration at time $t + \Delta t$, whereas $^{t}\square$ is the configuration at time t. For simplicity, we will <u>omit</u> the left superscript for the current configuration, i.e., $\square \equiv {}^{t+\Delta t}\square$. A comma followed by a subscript variable x_i denotes a partial derivative with respect to that subscript variable (i.e. $f_{,x_i} \equiv \partial f / \partial x_i$). Summation convention for repeated subscripts is employed. Subscript pairs with regular and square parentheses denote the symmetric and antisymmetric gradients, respectively. The material time derivative is denoted by a superposed dot. For example, $v_i = \dot{x}_i$ is the velocity component; and the components of the rate of deformation, $\dot{\varepsilon}_{ij}$, and spin, $\dot{\omega}_{ij}$, are defined as

$$\dot{\varepsilon}_{ij} \equiv v_{(i, x_j)} = \frac{1}{2}\left(\frac{\partial v_i}{\partial x_j} + \frac{\partial v_j}{\partial x_i}\right) \qquad \dot{\omega}_{ij} \equiv v_{[i, x_j]} = \frac{1}{2}\left(\frac{\partial v_i}{\partial x_j} - \frac{\partial v_j}{\partial x_i}\right) \tag{1}$$

We consider a class of finite-deformation constitutive equations in the rate form commonly used in computational plasticity:

$$\dot{\sigma}_{ij} = \overset{\circ}{\sigma}_{ij} + \hat{\sigma}_{ij} \qquad \text{where} \qquad \hat{\sigma}_{ij} = \dot{\Lambda}_{ik}\sigma_{kj} - \sigma_{ik}\dot{\Lambda}_{kj} \tag{2}$$

where σ_{ij} represents the Cauchy stress; $\overset{\circ}{\sigma}_{ij}$ is an objective rate of Cauchy stress, which represents the material response due to deformation; $\dot{\Lambda}_{ij} = \dot{R}_{ik}R_{kj}^{-1}$ represents the rate of rotation R_{ij}. We refer to [2] for a comprehensive discussion on various choices of R_{ij} and $\dot{\Lambda}_{ij}$. For subsequent discussion we consider the choice: $\dot{\Lambda}_{ij} = \dot{\omega}_{ij}$.

We adopt an additive split of the rate of deformation, $\dot{\varepsilon}_{ij}$, into elastic rate of deformation, $\dot{\varepsilon}_{ij}^e$, and plastic rate of deformation, $\dot{\varepsilon}_{ij}^p$, which gives

$$\dot{\varepsilon}_{ij} = \dot{\varepsilon}_{ij}^e + \dot{\varepsilon}_{ij}^p, \qquad \overset{\circ}{\sigma}_{ij} = L_{ijkl}(\dot{\varepsilon}_{kl} - \dot{\varepsilon}_{kl}^p) \tag{3}$$

where L_{ijkl} are components of the elastic constitutive tensor.

We consider the yield function Φ defined by:

$$\Phi(\sigma_{ij}, \alpha_{ij}, Y) = \frac{1}{2}(\sigma_{ij} - \alpha_{ij})P_{ijkl}(\sigma_{kl} - \alpha_{kl}) - \frac{1}{3}Y^2 \tag{4}$$

where Y is the yield stress; α_{ij} the back stress corresponding to the center of the yield surface in the deviatoric stress space; P_{ijkl} the projection operator, satisfying $P_{ijkl}P_{klmn} = P_{ijmn}$. For von Mises plasticity the projection operator is defined as follows:

$$P_{ijkl} = I_{ijkl} - \frac{1}{3}\delta_{ij}\delta_{kl} \qquad \text{where} \qquad I_{ijkl} = \frac{1}{2}(\delta_{ik}\delta_{jl} + \delta_{il}\delta_{jk}) \tag{5}$$

and δ_{ij} is the Kronecker delta. For simplicity we assume the associative flow rule

$$\dot{\varepsilon}_{ij}^p = \frac{\partial \Phi}{\partial \sigma_{ij}}\dot{\lambda} = \aleph_{ij}\dot{\lambda} \qquad \text{where} \qquad \aleph_{ij} = P_{ijkl}(\sigma_{kl} - \alpha_{kl}) \tag{6}$$

and λ is a plastic parameter to be determined by plastic consistency condition (4). The evolution of the yield stress and the back stress are given in the rate form:

$$\dot{Y} = \frac{2\beta H}{3}Y\dot{\lambda} \tag{7}$$

$$\overset{\circ}{\alpha}_{ij} = \frac{2(1-\beta)H}{3}P_{ijkl}(\sigma_{kl} - \alpha_{kl})\dot{\lambda} \tag{8}$$

where β is a material dependent parameter, $(0 \leq \beta \leq 1)$. The extreme values $\beta = 0$ and $\beta = 1$ refer to Ziegler-Prager kinematic and pure isotropic hardening, respectively; H is a hardening parameter defining the ratio between the rate of effective stress and the rate of effective plastic strain.

3.0 Integration of rate constitutive equations

In this section, we briefly outline the Hughes-Winget incrementally objective integration scheme [3] in the context of finite deformation analysis in which the stress objectivity is

preserved for finite rotation increments. We then briefly summarize the closest point projection scheme closely related to radial return algorithms for integrating material response [2], [5], [6].

3.1 Incrementally objective integration algorithms

There are several incrementally objective integration schemes. One of the most popular approaches is known as the corotational method, where all the fields of interest are transformed into the corotational system [2], [10]. In such a corotational system, the form of constitutive equations is analogous to that of small deformation theory and is consistent with the generalized notion of hyperelasticity provided that an appropriate choice of the rotation tensor, R, is made [9]. An alternative approach developed by Hughes and Winget [3] is based on the additive incremental split of material and rotational response. In the present manuscript we focus on the latter.

The Hughes-Winget algorithm [3], for integrating the rate constitutive equations arising from the finite deformation can be summarized as follows:

$$\sigma_{ij} \equiv {}^{t+\Delta t}\sigma_{ij} = {}^{t}\hat{\sigma}_{ij} + \Delta\sigma_{ij}, \qquad {}^{t}\hat{\sigma}_{ij} = R_{ik}\,{}^{t}\sigma_{kl}\,R_{jl} \qquad (9)$$

$$\alpha_{ij} \equiv {}^{t+\Delta t}\alpha_{ij} = {}^{t}\hat{\alpha}_{ij} + \Delta\alpha_{ij}, \qquad {}^{t}\hat{\alpha}_{ij} = R_{ik}\,{}^{t}\alpha_{kl}\,R_{jl} \qquad (10)$$

where $\Delta\sigma_{ij}$ and $\Delta\alpha_{ij}$ denote the stress and back stress increments resulting from the material response (see Section 3.2), and R_{ij} is obtained by applying the generalized midpoint rule [3]:

$$R_{ij} = \delta_{ij} + \left(\delta_{ik} - \frac{1}{2}\Delta\omega_{ik}\right)^{-1}\Delta\omega_{kj} \qquad (11)$$

To maintain the second order accuracy [3] strain and rotation increments are obtained using the midpoint rule:

$$\Delta\varepsilon_{ij} = \frac{1}{2}\left(\frac{\partial\Delta u_i}{\partial^{t+\Delta t/2}x_j} + \frac{\partial\Delta u_j}{\partial^{t+\Delta t/2}x_i}\right), \qquad \Delta\omega_{ij} = \frac{1}{2}\left(\frac{\partial\Delta u_i}{\partial^{t+\Delta t/2}x_j} - \frac{\partial\Delta u_j}{\partial^{t+\Delta t/2}x_i}\right) \qquad (12)$$

where Δu_i is a displacement increment component and

$$^{t+\Delta t}x_i = {}^t x_i + \Delta u_i, \qquad {}^{t+\Delta t/2}x_i \equiv \frac{1}{2}({}^t x_i + {}^{t+\Delta t}x_i) \tag{13}$$

3.2 Closest point projection scheme

For integrating the material response given in the rate form ((6), (7), (8)), the Backward Euler integration scheme, which can be interpreted as the closest point projection algorithm [5], is employed:

$$\varepsilon_{ij}^p = {}^t\varepsilon_{ij}^p + \aleph_{ij}\Delta\lambda \tag{14}$$

$$Y = {}^tY + \frac{2\beta H}{3}Y\Delta\lambda \quad \Rightarrow \quad Y = \frac{3\,{}^tY}{3 - 2\beta H\Delta\lambda} \tag{15}$$

$$\alpha_{ij} = {}^t\hat{\alpha}_{ij} + \frac{2(1-\beta)H}{3}P_{ijkl}(\sigma_{kl} - \alpha_{kl})\Delta\lambda \tag{16}$$

$$\sigma_{ij} = \sigma_{ij}^{tr} - L_{ijkl}\aleph_{kl}\Delta\lambda, \quad \sigma_{ij}^{tr} = {}^t\hat{\sigma}_{ij} + L_{ijkl}\Delta\varepsilon_{kl} \tag{17}$$

where $\Delta\lambda \equiv {}^{t+\Delta t}\lambda - {}^t\lambda$

The process is regarded elastic if:

$$\left.(\sigma_{ij}^{tr} - \alpha_{ij})P_{ijkl}(\sigma_{kl}^{tr} - \alpha_{kl}) - \frac{2}{3}Y^2\right|_{\Delta\lambda^{(m)} = 0} < 0 \tag{18}$$

Otherwise the process is plastic. In the case of the plastic process we proceed by subtracting (16) from (17) to arrive at the following result:

$$\sigma_{ij} - \alpha_{ij} = (I_{ijkl} + \Delta\lambda\,\wp_{ijkl})^{-1}(\sigma_{kl}^{tr} - {}^t\hat{\alpha}_{kl}) \tag{19}$$

where

$$\wp_{ijkl} = L_{ijst}P_{stkl} + \frac{2}{3}(1-\beta)HP_{ijkl} \tag{20}$$

The value of $\Delta\lambda$ is obtained by satisfying the consistency condition (4). Substituting (15) and (19) into (4) produces a nonlinear equation for $\Delta\lambda$. The Newton method is typically used to solve for $\Delta\lambda$:

$$\Delta\lambda_{k+1} = \Delta\lambda_k - \left\{ \frac{\partial\Phi}{\partial\Delta\lambda} \right\}^{-1} \Phi \Bigg|_{\Delta\lambda_k} \tag{21}$$

where k is the iteration count. It can be shown that the derivative $\partial\Phi/\partial\Delta\lambda$ required in (21) is given as:

$$\frac{\partial\Phi}{\partial\Delta\lambda} = -\aleph_{ij}(I_{ijkl} + \Delta\lambda\,\wp_{ijkl})^{-1}\wp_{klmn}(\sigma_{mn} - \alpha_{mn}) - \frac{4\beta h Y^2}{9 - 6\beta h\Delta\lambda} \tag{22}$$

The converged value of $\Delta\lambda$ is then used in combination with (19), (15), (16) and (17) to update the yield stress, the back stress, and the Cauchy stress.

4.0 Consistent linearization

While integration of the constitutive equations affects the accuracy of the solution, the formulation of the tangent stiffness matrix consistent with the integration procedure employed is essential to maintain the asymptotic quadratic rate of convergence of the Newton method provided that the solution is smooth. In Section 4.1 we derive the Jacobian matrix for the finite deformation elasto-plastic constitutive model, which in Section 4.2 leads to the formulation of the tangent stiffness matrix consistent with the integration procedures outlined in Section 3.

4.1 The Jacobian matrix for the finite deformation elasto-plastic constitutive model

The Jacobian matrix for the finite deformation elasto-plastic constitutive model outlined in the previous sections is obtained by taking the material time derivative of the stress and the back stress ((17), (16)) at the current configuration (time $t + \Delta t$):

$$\dot{\sigma}_{ij} = {}^{t}\hat{\dot{\sigma}}_{ij} + L_{ijkl}\{\Delta\dot{\varepsilon}_{kl} - P_{klmn}(\dot{\sigma}_{mn} - \dot{\alpha}_{mn})\Delta\lambda - \aleph_{kl}\dot{\lambda}\} \tag{23}$$

$$\dot{\alpha}_{ij} = {}^{t}\hat{\dot{\alpha}}_{ij} + \frac{2(1-\beta)h}{3}\{P_{ijpq}(\dot{\sigma}_{pq} - \dot{\alpha}_{pq})\Delta\lambda + \aleph_{ij}\dot{\lambda}\} \tag{24}$$

Remark 1: It is common in practice (see for example Section 3.2.2 in ABAQUS theory manual [12]) to introduce the following two approximations, which assume infinitesimality of the time step:

$$\overset{t}{\hat{\sigma}}_{ij} \approx \hat{\sigma}_{ij} = \Lambda_{ik}\sigma_{kj} - \sigma_{ik}\Lambda_{kj} \qquad \Delta\dot{\varepsilon}_{kl} \approx \dot{\varepsilon}_{kl} \tag{25}$$

In the remainder of this section we derive the consistent Jacobian matrix exactly, and in Section 5, we show that the two approximations given in (25) considerably increase the number of iterations in the Newton method.

We start by subtracting (24) from (23) which yields:

$$\dot{\sigma}_{ij} - \dot{\alpha}_{ij} = (I_{ijkl} + \Delta\lambda\,\wp_{ijkl})^{-1}\left\{(\overset{t}{\hat{\sigma}}_{kl} - \overset{t}{\hat{\alpha}}_{kl}) + L_{klmn}\Delta\dot{\varepsilon}_{mn} - \wp_{klmn}\aleph_{mn}\dot{\lambda}\right\} \tag{26}$$

where $\overset{t}{\hat{\sigma}}_{ij}$ and $\overset{t}{\hat{\alpha}}_{ij}$ in (26) are computed by taking the material time derivative of (9) and (10), which yields

$$\overset{t}{\hat{\sigma}}_{ij} = A^{\sigma}_{ijmn}\dot{R}_{mn}, \qquad \overset{t}{\hat{\alpha}}_{ij} = A^{\alpha}_{ijmn}\dot{R}_{mn} \tag{27}$$

where

$$A^{\sigma}_{ijmn} = (\delta_{im}\delta_{kn}R_{jl} + \delta_{jm}\delta_{nl}R_{ik})\,^{t}\sigma_{kl}$$
$$A^{\alpha}_{ijmn} = (\delta_{im}\delta_{kn}R_{jl} + \delta_{jm}\delta_{nl}R_{ik})\,^{t}\alpha_{kl} \tag{28}$$

Taking the material derivative of (11) gives

$$\dot{R}_{mn} = B_{mnpq}\Delta\dot{\omega}_{pq} \tag{29}$$

where

$$B_{mnpq} = (2\delta_{mp} - \Delta\omega_{mp})^{-1}(\delta_{qn} + R_{qn}) \tag{30}$$

Substituting (29) into (27) results in

$$\overset{t}{\hat{\sigma}}_{ij} - \overset{t}{\hat{\alpha}}_{ij} = T_{(ij)[pq]}\Delta\dot{\omega}_{pq} \tag{31}$$

where

$$T_{ijpq} = (A^{\sigma}_{ijmn} - A^{\alpha}_{ijmn})B_{mnpq} \tag{32}$$

It is important to note that the derivation of $\Delta\dot{\varepsilon}_{ij}$ and $\Delta\dot{\omega}_{ij}$ appearing in equations (26) and (31), should be consistent with the midpoint integration scheme employed. In the following we focus on such consistent linearization.

We start by taking the material time derivative of the gradient of the displacement increment with respect to the position vector at the midstep (see equation (12)):

$$\frac{d}{dt}\left(\frac{\partial\Delta u_i}{\partial^{t+\Delta t/2}x_j}\right) = \frac{\partial v_i}{\partial^t x_k}\frac{\partial^t x_k}{\partial^{t+\Delta t/2}x_j} + \frac{\partial\Delta u_i}{\partial^t x_k}\frac{d}{dt}\left(\frac{\partial^t x_k}{\partial^{t+\Delta t/2}x_j}\right) \tag{33}$$

Linearization of the second term in (33) yields

$$\frac{d}{dt}\left(\frac{\partial^t x_k}{\partial^{t+\Delta t/2}x_j}\right) = -\frac{\partial^t x_k}{\partial^{t+\Delta t/2}x_m}\frac{d}{dt}\left(\frac{\partial^{t+\Delta t/2}x_m}{\partial^t x_n}\right)\frac{\partial^t x_n}{\partial^{t+\Delta t/2}x_j} \tag{34}$$

Combining (33) and (34) gives

$$\frac{d}{dt}\left(\frac{\partial\Delta u_i}{\partial^{t+\Delta t/2}x_j}\right) = \frac{\partial v_i}{\partial^{t+\Delta t/2}x_j} - \frac{\partial\Delta u_i}{\partial^{t+\Delta t/2}x_m}\frac{d}{dt}\left(\frac{\partial^{t+\Delta t/2}x_m}{\partial^t x_n}\right)\frac{\partial^t x_n}{\partial^{t+\Delta t/2}x_j} \tag{35}$$

Equation (35) can be further simplified by exploiting the following relation

$$\frac{d}{dt}\left(\frac{\partial^{t+\Delta t/2}x_m}{\partial^t x_n}\right) = \frac{\partial}{\partial^t x_n}\left(\frac{d}{dt}{}^{t+\Delta t/2}x_m\right) = \frac{\partial}{\partial^t x_n}\left\{\frac{d}{dt}\left(\frac{x_m + {}^t x_m}{2}\right)\right\} = \frac{1}{2}\frac{\partial v_m}{\partial^t x_n} \tag{36}$$

which after substitution into (35) yields

$$\frac{d}{dt}\left(\frac{\partial\Delta u_i}{\partial^{t+\Delta t/2}x_j}\right) = \left(\delta_{im} - \frac{1}{2}\frac{\partial\Delta u_i}{\partial^{t+\Delta t/2}x_m}\right)\frac{\partial v_m}{\partial^{t+\Delta t/2}x_j} \tag{37}$$

By utilizing the following equality

$$\delta_{im} - \frac{1}{2} \frac{\partial \Delta u_i}{\partial^{t+\Delta t/2} x_m} = \frac{\partial}{\partial^{t+\Delta t/2} x_m}\left(^{t+\Delta t/2} x_i - \frac{1}{2}\Delta u_i\right) = \frac{\partial^t x_i}{\partial^{t+\Delta t/2} x_m} \tag{38}$$

equation (37) can be recast into the following form:

$$\frac{d}{dt}\left(\frac{\partial \Delta u_i}{\partial^{t+\Delta t/2} x_j}\right) = \frac{\partial^t x_i}{\partial^{t+\Delta t/2} x_m} \frac{\partial v_m}{\partial^{t+\Delta t/2} x_j} \tag{39}$$

Defining M_{ijkl} as

$$M_{ijkl} \equiv \frac{\partial^t x_i}{\partial^{t+\Delta t/2} x_k} \frac{\partial x_l}{\partial^{t+\Delta t/2} x_j} \tag{40}$$

yields

$$\frac{d}{dt}\left(\frac{\partial \Delta u_i}{\partial^{t+\Delta t/2} x_j}\right) = M_{ijkl} \, v_{k,x_l} \tag{41}$$

Taking symmetric and antisymmetric part of (41) with respect to indexes ij we get the final expressions for $\Delta \dot{\varepsilon}_{ij}$ and $\Delta \dot{\omega}_{ij}$:

$$\Delta \dot{\varepsilon}_{ij} = M_{(ij)kl} \, v_{k,x_l}, \qquad \Delta \dot{\omega}_{ij} = M_{[ij]kl} \, v_{k,x_l} \tag{42}$$

It can be easily seen that for infinitesimally small step size $M_{ijkl} = \delta_{ik}\delta_{jl}$.

We proceed by substituting (42) and (31) into (26), which yields

$$\dot{\sigma}_{ij} - \dot{\alpha}_{ij} = (I_{ijkl} + \Delta\lambda \wp_{ijkl})^{-1}\{L^e_{klmn} v_{m,x_n} - \wp_{klmn} \aleph_{mn}\dot{\lambda}\} \tag{43}$$

where L^e_{klmn} is the Jacobian matrix for the finite deformation elastic constitutive model given as

$$L^e_{klpq} = T_{klmn}M_{[mn]pq} + L_{klmn}M_{(mn)pq} \tag{44}$$

The plastic parameter, $\hat{\lambda}$, in (43) is computed by linearizing consistency condition (4), i.e. $\dot{\Phi} = 0$, which yields

$$\aleph_{ij}(\dot{\sigma}_{ij} - \dot{\alpha}_{ij}) - \frac{4\beta HY^2 \dot{\lambda}}{9 - 6\beta H\Delta\lambda} = 0 \tag{45}$$

Substituting (43) into (45) provides

$$\dot{\lambda} = S_{mn} v_{m,n} \tag{46}$$

where

$$S_{mn} = \frac{\aleph_{ij}(I_{ijkl} + \Delta\lambda \wp_{ijkl})^{-1} L^e_{klmn}}{\aleph_{ij}(I_{ijkl} + \Delta\lambda \wp_{ijkl})^{-1} \wp_{klpq} \aleph_{pq} + \dfrac{4\beta HY^2}{9 - 6\beta H\Delta\lambda}} \tag{47}$$

The Jacobian matrix for the finite deformation plastic constitutive model, L^p_{ijkl}, is obtained by substituting (46), (27) and (29) into (23), which yields

$$\dot{\sigma}_{ij} = L^p_{ijkl} v_{k,x_l} \tag{48}$$

where

$$
\begin{aligned}
L^p_{ijkl} = {} & A^\sigma_{ijmn} B_{mnpq} M_{[pq]kl} + \\
& L_{ijmn}\left\{ M_{(mn)kl} - P_{mnpq}\left(\frac{I_{pqst}}{\Delta\lambda} + \wp_{pqst}\right)^{-1}(L^e_{stkl} - \wp_{stuv}\aleph_{uv}S_{kl}) - \aleph_{mn}S_{kl}\right\}
\end{aligned}
\tag{49}
$$

Finally, the Jacobian matrix for the finite deformation elasto-plastic constitutive model is given as

$$L_{ijkl} = \begin{cases} L^e_{ijkl} & \text{for elastic process} \\ L^p_{ijkl} & \text{for plastic process} \end{cases} \tag{50}$$

4.2 Consistent tangent stiffness matrix

We start from the system of nonlinear equations arising from the finite element discretization

$$r_A = f_A^{int}(q_A) - f_A^{ext} = 0 \qquad f_A^{int} = \int_\Omega N_{iA, x_j} \sigma_{ij} d\Omega \tag{51}$$

where N_{kA} is set of C^0 continuous shape functions, such that $v_k = N_{kA} \dot{q}_A$; the upper case subscripts denote the degree-of-freedom and the summation convention over repeated indexes is employed for the degrees-of-freedom and for the spatial dimensions; q_A and $\dot{q}_A$ are components of nodal displacement and velocity vectors; and f_A^{int} and f_A^{ext} are components of the internal and external force vectors, respectively.

The consistent tangent stiffness matrix, K_{AB}, is obtained via consistent linearization of the discrete equilibrium equations (51). It is convenient to formulate such a linearization procedure as:

$$K_{AB} \equiv \frac{\partial}{\partial \dot{q}_B}\left(\frac{d}{dt} r_A\right) \tag{52}$$

For simplicity, assuming that the external force vector is not a function of the solution, the consistent linearization procedure yields:

$$\frac{d}{dt} r_A = \int_{{}^t\Omega} \frac{d}{dt}(N_{iA,\,{}^tx_m} F_{mj}^{-1} \sigma_{ij} J) d^t\Omega \tag{53}$$

where J is the Jacobian between the configurations t and $t + \Delta t$; F_{jm} is the deformation gradient defined as

$$F_{jm} = x_{j,\,{}^tx_m} \equiv {}^{t+\Delta t}x_{j,\,{}^tx_m} \qquad \text{and} \qquad F_{mj}^{-1} = {}^tx_{m, x_j} \equiv {}^tx_{m,\,{}^{t+\Delta t}x_j} \tag{54}$$

Linearization of (53) yields

$$\frac{d}{dt} r_A = \int_{{}^t\Omega} N_{iA,\,{}^tx_m} \{\dot{F}_{mj}^{-1} \sigma_{ij} J + F_{mj}^{-1} \dot{\sigma}_{ij} J + F_{mj}^{-1} \sigma_{ij} \dot{J}\} d^t\Omega \tag{55}$$

Substituting (50) into (55) and exploiting the well-known kinematical relations $\dot{J} = J v_{k, x_k}$, $\dot{F}_{mj}^{-1} = -F_{ml}^{-1} v_{l, x_j}$ yields:

$$K_{AB} = \int_{\Omega} N_{iA,\,x_j} \bar{L}_{ijkl} N_{kB,\,x_l}\, d\Omega \qquad (56)$$

where

$$\bar{L}_{ijkl} = L_{ijkl} + \delta_{kl}\sigma_{ij} - \delta_{kj}\sigma_{il} \qquad (57)$$

and L_{ijkl} is defined in (50).

5.0 Numerical experiments

Numerical integration and consistent linearization schemes described in sections 4 and 5 have been implemented into ABAQUS [12] as a User defined ELement (UEL). Note that in ABAQUS finite deformation plasticity algorithms are similar to those described in Section 4. The key difference is in the formulation of the tangent stiffness matrix. Hence while the solutions are (almost) identical, the iterative process would have a different character. Three numerical examples are considered. In the first (Section 5.1) we investigate the accuracy of the Hughes-Winget integration algorithm, whereas the following two subsections (5.2 and 5.3) focus on the computational efficiency aspects. For the numerical experiments considered in Sections 5.2 and 5.3, the load increments were chosen so that the total error resulting from the numerical integration will not exceed 3% in the maximal deflection.

5.1 Rotating-stretching bar problem

To investigate the accuracy of the integration algorithm, we consider a rotating-stretching bar problem [26]. The total rotation is 90°, whereas the total stretching is only 0.1%. The prescribed solution is applied in three increments, i.e., rotation increment is 30°. Figure 1 compares the accuracy of the Hughes-Winget integration algorithm with the higher order integration scheme [26] and the exact solution. It can be seen that even though rotation increments are very large, the second order accurate Hughes-Winget algorithm provides excellent accuracy in the stress field, resulting in the maximum error not exceeding 6%.
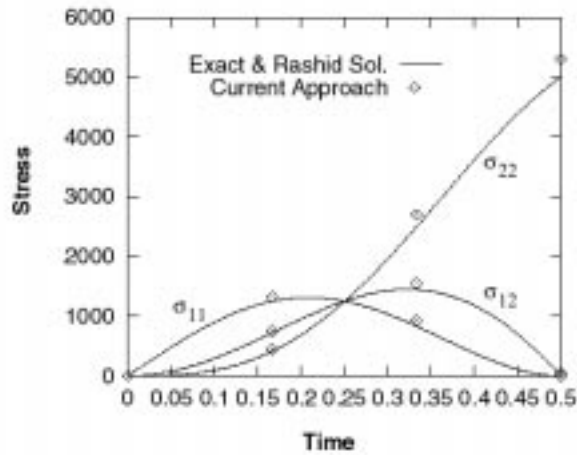
Figure 1: Rotating-stretching bar problem

5.2 Rigid body rotation of tetrahedral

In our second numerical experiment, we consider a single tetrahedral element subjected to a rigid body finite rotation. The initial and final configurations are shown in Figure 2.
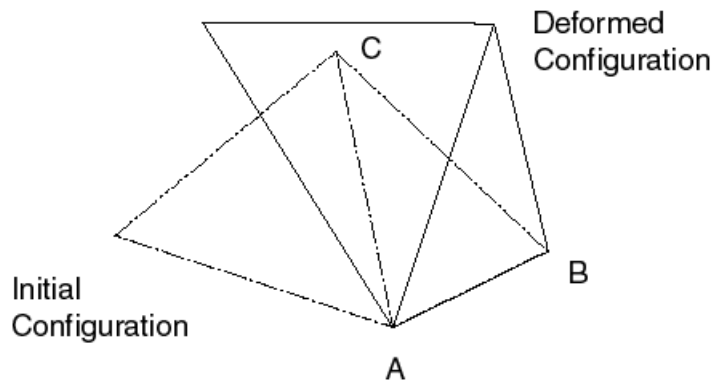

Figure 2: Rotation of tetrahedral element

The material is considered elastic with Young's modulus, $E = 21000$, the Poisson's ratio, $\nu = 0.3$. The boundary conditions are set in such a way that nodes A and B are held

fixed, while the horizontal component of the displacement at node C is prescribed, resulting in a rotation angle of approximately $40°$.

The prescribed displacement is applied in one increment, and it takes 5 iterations using consistent tangent and 54 iterations using approximate tangent (the original ABAQUS algorithm). With smaller load increments the advantage is less drastic. For example, for the same loading applied in three increments the number of iterations using the consistent tangent is 4, 5 and 5, whereas with the approximate tangent the number of iterations is 15, 16 and 16.

5.3 The 3D beam problem

We next consider a cantilever beam problem as shown in Figure 3. All the degrees-of-freedom at the clamped end are fixed. Uniform loading is applied at the tip of the beam in the transverse direction. The length, width, and the depth of the beam are 12, 1 and 2, respectively. The elastic constants are the same as in the previous example. Plasticity parameters are as follows: the hardening modulus, $H = 1000$, the mixed hardening parameter, $\beta = 1$, and the initial yield stress, $^0Y = 21$. The finite element mesh contains 4351 4-node tetrahedral elements totaling 1091 nodes. We consider two cases: an elastic beam (geometric nonlinearity only), and an elasto-plastic beam (geometric and material nonlinearity). In both cases the magnitude of loading is selected so that the maximal deflection at the tip is approximately one third of the beam length. For the problem with material nonlinearity 79% of elements experience plastic deformation.

The loading is applied in one increment. With the consistent tangent stiffness matrix the number of iterations is 11 and 16 for elastic and elasto-plastic problems, respectively. With the conventional tangent the number of iterations increases to 26 and 38 for elastic and elasto-plastic problems, respectively.

To this end we note that the computational cost of the consistent tangent stiffness matrix evaluation was approximately twice as high as that of the approximate tangent, but the

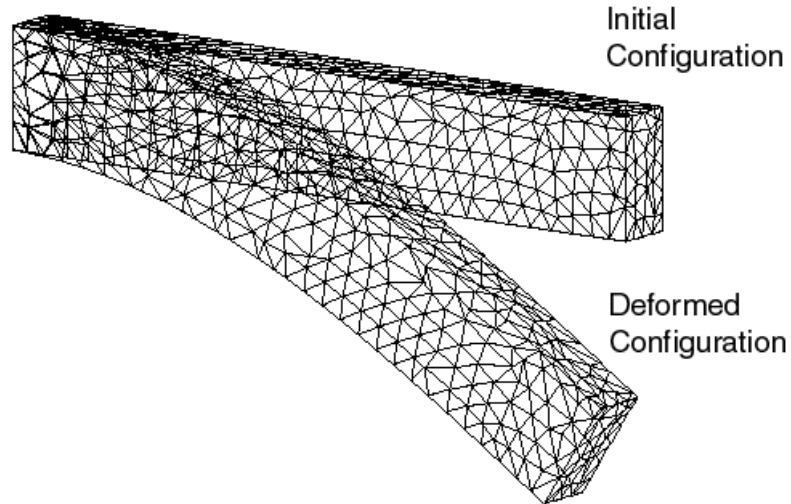overall computational cost associated with the formulation employing consistent tangent was still lower.

Figure 3: Deformation of cantilever beam

6.0 Summary and future research

A methodology for efficient implementation of the incrementally objective algorithm [3] has been developed. The usefulness of the proposed formulation has been demonstrated as the numerical experiments show significant savings in computational cost.

The scope of the paper was limited to the cases where the notion of hypoelasticity is valid. This is appropriate for metals, where elastic strains remain small compared to plastic deformation. For polymers, which exhibit large elastic and plastic deformations of comparable magnitude, a different treatment might be required.

Several questions, however, remained unanswered. First, we have not investigated whether a consistent tangent operator for the incrementally objective corotational formulation with the rotation part extracted from the deformation gradient can be derived with the same ease as for the present formulation. Such a corotational formulation would have a number of advantages, the key one being compatible with the notion of hyperelasticity [9]. Secondly, it is important to investigate how increasingly complex incrementally objective

algorithms would fare against the multiplicative decomposition and hyperelasticity based algorithms [8] in terms of accuracy and computational efficiency.

References

1   J. C. Nagtegaal, "On the implementation of inelastic constitutive equations with special reference to large deformation problems," *Computer Methods in Applied Mechanics and Engineering*, 33, 1982.

2   T. J. R. Hughes, "Numerical implementation of constitutive models: rate-independent deviatoric plasticity," in S. Nemat-Nasser, R. J. Asaro and G. A. Hegemier, editors, *Theoretical Foundation for Large Scale Computations for Nonlinear Material Behavior*, Martinus Nijhoff Publishers, 1983.

3   T. J. R. Hughes and J. Winget, "Finite rotation effects in numerical integration of rate constitutive equations arising in large deformation analysis," *International Journal of Numerical Methods in Engineering*, 15, 1980.

4   J. C. Simo and R. L. Taylor, "Consistent tangent operators for rate-independent elastoplasticity," *Computer Methods in Applied Mechanics and Engineering*, 48, 1985.

5   M. Ortiz and E.P. Popov, "Accuracy and stability of integration algorithms for elastoplastic constitutive equations," *International Journal of Numerical Methods in Engineering*, 21, 1985.

6   M. L. Wilkins, "Calculation of elastic-plastic flow," Methods in Computational Physics, Ed. B. Adler et al, Vol. 3, Academic Press, NY, 1964.

7   J. C. Simo, "A framework for finite strain elastoplasticity based on maximum plastic dissipation and the multiplicative decomposition. Part II: Computational aspects," *Computer Methods in Applied Mechanics and Engineering*, 68, 1988.

8   J. C. Simo and M. Ortiz, "A unified approach to finite deformation elasto-plastic analysis based on the use of hyperelastic constitutive tensor," *Computer Methods in Applied Mechanics and Engineering*, 49, 1985.

9   J. C. Simo and K.S. Pister, "Remarks on rate constitutive equations for finite deformation problems: computational implications," *Computer Methods in Applied Mechanics and Engineering*, 46, 1985.

10 T. Belytschko and B. J. Hsieh, "Nonlinear transient finite element analysis with convected coordinates," *International Journal of Numerical Methods in Engineering*, 7, 1973.

11 B. Moran, M.Ortiz and C.F. Shih, "Formulation of implicit finite element methods for multiplicative finite deformation plasticity," *International Journal of Numerical Methods in Engineering*, 29, 1990

12 ABAQUS Theory Manual, Version 5.4, Hibbit, Karlson & Sorensen, Inc., 1994.

13 S. Choudhry, S. Krishnaswami and T.B. Wertheimer, "Hyperelasticity based finite

strain plasticity algorithms in MARC," Proceedings of the Fourth US National Congress on Computational Mechanics, August 6-8, 1997.

14 O.O. Storaasli, VSS code, Computational Structures Branch, NASA Langley, 1996

15 O. Axelsson and V.A. Barker, '*Finite Element Solution of Boundary Value Problems*,' Academic Press, 1984.

16 J. Fish and R. Guttal, "Adaptive Solver for the p-version of Finite Element Method," *International Journal for Numerical Methods in Engineering,* Vol. 40, pp. 1767-1784, (1997).

17 J. Fish and A. Suvorov, "Automated Adaptive Multilevel Solver," *Comp. Meth. Appl. Mech. Engng*., Vol. 149, pp. 267-287, (1997)

18 V. Belsky and J. Fish, "Towards an ultimate finite element oriented solver on unstructured meshes," Proceedings of the Computers in Engineering Conference, ASME, September 17-20, 1995, Boston.

19 K. C. Parks and G. Stanley, "A curved Co shell element based on assumed natural coordinate strain," J. Appl. Mech., Vol. 108, (1986).

20 J.Fish and T.Belytschko, "Stabilized rapidly convergent shell element with drilling degrees-of-freedom," *International Journal for Numerical Methods in Engineering*, Vol. 33, pp. 149-162 (1992).

21 J. Fish and R. Guttal, "The p-version of finite element method for shell analysis," Computational Mechanics, Vol. 16, 328-340, 1995.

22 J. Fish and R. Guttal, "Adaptive solver for the p-version of finite element method," *International Journal for Numerical Methods in Engineering*, Vol. 40, pp. 1767-1784 (1997).

23 I. Babuska and T. Scapolla, "Computational aspects of the h, p, h-p versions of the finite element method," Advances in Computer Methods for Partial Differential Equations, VI, R. Vichnevetsky and R.S. Stepleman (Editors), IMACS publications, (1987)

24 H. P. Hackenberg, "Large deformation finite element analysis with inelastic constitutive models including damage," Computational Mechanics, Vol. 16, pp. 315-327, (1995)

25 B. Nour-Omid and C.C. Rankin, "Finite rotation and consistent linearization using projectors," *Computer Methods in Applied Mechanics and Engineering*, 93, pp. 353-384, 1991.

26 M. M. Rashid, "Incremental Kinematics for Finite Element Applications," *International Journal for Numerical Methods in Engineering*, Vol. 36, pp. 3937-3956 (1993).

27 R. I. Borja and E. Alarcon, "A mathematical framework for finite strain elastoplastic consolidation. Part 1: Balance laws, variational formulation, and linearization," *Computer Methods in Applied Mechanics and Engineering*, 122, pp. 145-171, (1995).